

Relationship between neural and hemodynamic signals during spontaneous activity studied with temporal kernel CCA

Yusuke Murayama^{a,*}, Felix Bießmann^b, Frank C. Meinecke^b, Klaus-Robert Müller^b,
Mark Augath^a, Axel Oeltermann^a, Nikos K. Logothetis^{a,c}

^aMax-Planck Institute for Biological Cybernetics, 72076 Tübingen, Germany

^bTU Berlin, Machine Learning Group, 10587 Berlin, Germany

^cDivision of Imaging Science and Biomedical Engineering, University of Manchester, M13 9PT, Manchester, UK

Received 10 October 2009; revised 6 December 2009; accepted 7 December 2009

Abstract

Functional magnetic resonance imaging (fMRI) based on the so-called blood oxygen level-dependent (BOLD) contrast is a powerful tool for studying brain function not only locally but also on the large scale. Most studies assume a simple relationship between neural and BOLD activity, in spite of the fact that it is important to elucidate how the “when” and “what” components of neural activity are correlated to the “where” of fMRI data. Here we conducted simultaneous recordings of neural and BOLD signal fluctuations in primary visual (V1) cortex of anesthetized monkeys. We explored the neurovascular relationship during periods of spontaneous activity by using temporal kernel canonical correlation analysis (tkCCA). tkCCA is a multivariate method that can take into account any features in the signals that univariate analysis cannot. The method detects filters in voxel space (for fMRI data) and in frequency–time space (for neural data) that maximize the neurovascular correlation without any assumption of a hemodynamic response function (HRF). Our results showed a positive neurovascular coupling with a lag of 4–5 s and a larger contribution from local field potentials (LFPs) in the γ range than from low-frequency LFPs or spiking activity. The method also detected a higher correlation around the recording site in the concurrent spatial map, even though the pattern covered most of the occipital part of V1. These results are consistent with those of previous studies and represent the first multivariate analysis of intracranial electrophysiology and high-resolution fMRI.

© 2010 Elsevier Inc. All rights reserved.

Keywords: BOLD; Local field potential; Multi-unit activity; Spontaneous activity; Hemodynamic response function; Canonical correlation; Monkey; Visual cortex

1. Introduction

Functional magnetic resonance imaging (fMRI) has been used extensively to map the physiological properties of various brain regions. Currently, fMRI relies on acquisition methods (i.e. pulse sequences) that enhance the so-called blood oxygen level-dependent (BOLD) contrast [1]. Since the BOLD contrast is a surrogate signal reflecting oxygenation changes due to neural activity rather than neural activity itself, it is of paramount importance to understand in depth which neural elements and processes actually contribute to the observed spatiotemporal changes in oxygenation. Not surprisingly, an ever increasing number

of studies are devoted to examining the relationship of the BOLD signal to the underlying neural activity using a variety of techniques [2–4].

In the vast majority of such studies investigators examine the statistical dependence between intracranially, transdually or extracranially (e.g. by means of electroencephalography) measured neural responses and BOLD dynamics. The functional maps obtained with BOLD contrast are commonly generated by studying the temporal dynamics of a very large set of points, termed *voxel elements* or *voxels*, in a three-dimensional space (multiple slices of the brain). In other words, the BOLD responses are multivariate with a very large number of dimensions (voxels). Due to this high dimensionality, standard fMRI analyses treat the time evolution of each voxel separately (a mass-univariate approach), assuming statistical independence between them

* Corresponding author. Tel.: +49 7071 601 663; fax: +49 7071 601 652.

E-mail address: yusuke.murayama@tuebingen.mpg.de (Y. Murayama).

and merely applying appropriate corrections for multiple comparisons (e.g., the Bonferroni correction). Yet dependencies between voxels are never negligible, nor are they uniform; voxels within a region of a functionally specialized brain area may be highly intercorrelated, while the borders of such regions may show correlations that are minimal to nonexistent. Moreover, the onset of the BOLD response with respect to the neural change and the response's time to peak are anything but constant and can vary significantly from voxel to voxel and from area to area. The exact time lag between neural and BOLD signals is poorly understood and can even vary across voxels and subjects [5]. Nonetheless, mass-univariate approaches commonly assume a peak delay of 5 s and usually approximate the vascular responses as the neural time series convolved by a fixed-width hemodynamic response function (HRF) that is implicitly considered to be of a cardinal nature (i.e. space invariant). In fact, no such cardinal HRF exists, which can be assumed for all cortical areas and all subjects [2–4,6]. Therefore, there is a real need for methodologies that are truly multivariate and sensitive to potential time differences between the neural and vascular onsets of activity. Not surprisingly, a number of multivariate analysis methods have recently been introduced as alternatives to mass-univariate methods (for a review and comparison, see, e.g., Ref. [7,8]).

In the present paper, we report on the application of one multivariate method which can simultaneously estimate the spatial and temporal dependencies between various components of the neural signal and the hemodynamic responses for the study of spontaneous activity in the visual cortex. More specifically, we employed a recently developed statistical learning technique termed *temporal kernel canonical correlation analysis (tkCCA)* [9] that estimates a filter for a frequency–time representation of neural signals and a multivariate fMRI time series, respectively. The filters are optimized to maximize the canonical correlation between the two sets of signals. tkCCA performs a maximization of the canonical correlation between two matrices as a whole and optimizes two weight filters for each matrix, taking into account any features represented in the data which can contribute to higher correlation.

The application of this method to simultaneous physiological and fMRI recordings within a subregion of the primary visual cortex during spontaneous activity yielded results that, overall, are similar to those obtained with standard correlation analysis. However, the activations mapped with tkCCA were restricted to the gray matter, and the computed correlations were consistently higher. More importantly, the analysis method did not depend on specific impulse response functions or spatial dependencies. This data-driven and assumption-free approach is likely to offer interesting insights when the neural responses recorded by electrodes placed in one area are compared with BOLD signals from different cortical areas, each of which is likely to have a different structure of correlation to the recorded neural signal.

2. Methods

2.1. Preparative surgery and experimental procedure

This study involved nine combined electrophysiological fMRI experiments in four healthy monkeys (*Macaca mulatta*) weighing 7–10 kg. All experiments and surgical procedures were approved by the local authorities (Regierungspräsidium) and were in full compliance with the guidelines of the European Community (EUVD 86/609/EEC) for the care and use of laboratory animals. A custom-made plastic head holder and a recording chamber were implanted directly on to the skull of each animal under general anesthesia (balanced anesthesia consisting of isoflurane 1.3% and fentanyl 3 µg/kg, iv, as needed).

The experiments were conducted under general anesthesia. After premedication with glycopyrrolate (0.01 mg/kg, im) and ketamine (15 mg/kg, im), the animals were preoxygenated and then intubated after induction with fentanyl (3 µg/kg, iv), thiopental (5 mg/kg, iv) and succinyl chloride (3 mg/kg, iv); they were artificially ventilated (Servo Ventilator 900C; Siemens, Germany), maintaining an end-tidal CO₂ of 33 mmHg and oxygen saturation of over 95%. Anesthesia was maintained with remifentanyl (0.5–2 µg/kg, iv) and muscle relaxation was achieved with mivacurium (3–6 mg/kg per hour, iv). Body temperature was kept at 38–39.5°C; lactated Ringer's solution (2.5% glucose) was infused at 10 ml/kg per hour, iv.

Drops of 1% cyclopentolate hydrochloride were instilled into each eye to achieve mydriasis, and hard contact lenses (Zeiss) with the appropriate dioptric power were used to bring the eyes to focus on the stimulus plane. Visual stimuli were presented binocularly using XGA fiberoptic projectors (Silent Vision; AVOTEC, Stuart, FL). Fiber scopes were aligned to the fovea of each of the subject's eyes using a modified fundus camera (RC250; Zeiss). The visual field of the scope was 30°×23°. Visual stimuli were generated on the fly with an OpenGL-based custom program. Stimulus timings and neuronal recordings were synchronized with MR image acquisition and controlled by a network-connected PC running a custom-made program under the QNX real-time OS [10].

2.2. fMRI and electrophysiological recording

We made measurements in a vertical 4.7-T scanner with a 40-cm-diameter bore (BioSpec 47/40v; Bruker Medical, Ettlingen, Germany) as described in detail previously [11]. Small, customized radiofrequency coils (30–80 mm diameter) were used to increase the sensitivity for the MR signal underneath a recording chamber. The multichannel electrodes were positioned using a gradient echo sequence with a field of view (FOV) of 96×96 mm in a matrix of 256×256 and a slice thickness of 1 mm. Multislice fMRI was carried out with multishot (segmented) GE-EPI. Before collecting spontaneous activity data, we ran a preliminary scan with full field visual stimulation to test whether BOLD and neural

signals were responsive. fMRI acquisition parameters were: FOV 64×64 or 96×96 mm; 7 or 12 slices (2 mm thickness); matrix size 64×64 or 96×96; 4 segments; echo time 15–20 ms; repetition time 250–500 ms; flip angle 20–40°; sweep width 100 kHz; 4–8 s dummy scanning. For anatomical reference, a FLASH sequence was carried out with the same FOV and slice angle as the fMRI slices but with double the matrix size and 0.5–1 mm slice thickness.

A small craniotomy was made at the beginning of each experiment to position the MRI-compatible multichannel electrode in early visual areas V1 and V2. The electrode was recently developed in-house and had a carrier made of carbon composites (300×300 μm cross section), Pt/Ir (90/10) wires (18 μm diameter; California Fine Wire, USA) embedded in and glued to the carrier for 10 contact sites in the brain, and flattened Ag wires glued to the carbon shaft as ground and interference sensor in the recording chamber. Procedures based on current measurement for signal amplification and noise minimization during simultaneous recordings are described in detail elsewhere [11,12]. The interference caused by the alternating magnetic field gradients during fMRI has two major components; the *far* interference, which can be reduced by adjusting the counter-current injection through a junction electrode (Ag wire) placed in the mouth, and the *near* interference, which is not measurable because it is too close to the recording site to permit the placement of additional sensors. This component can be approximated by a linear sum of gradient magnetic field changes in the XYZ directions and minimized within the preamplifier by adjusting each XYZ factor. For our multichannel electrode, *far*-interference compensation was done using a separate device for each channel, while *near*-interference compensation was done within each channel amplifier. For data collection, 4 out of 10 channels were selected as visually responsive channels by using a computer-controlled receptive field plotting program.

Amplified electrophysiological data were digitized with a 16bit AD card (PCI-6052E; National Instruments) at 20.83 kHz to collect broadband neural activities including local field potential, spiking activities and residual interference noise. For all measurements of spontaneous fluctuations, the eyes were kept open in darkness, with the stimulus projectors powered off to avoid the effects of LCD flicker [13].

All imaging and recording data were collected as blocks of 5-min scans. The test scan used to examine the BOLD and neural responses had 10 trials of blank–stimulus–blank/10–6–14 s. Polar gratings (100% contrast, rotating in a whole field) were presented as visual stimulation. A total of 30–60 min of spontaneous data in each session were used for data analysis.

2.3. Data analysis

Data analysis was done using custom-written software in MATLAB (The MathWorks, Natick, MA, USA).

In order to avoid different image intensities in scans, each voxel in the scan was normalized by dividing by the mean value of all voxels having enough intensity and multiplied by a user value of 1000. After this ratio-normalization, voxel data were spatially (*XY*) filtered with a Gaussian kernel (3×3 pixels with 1.5 sigma), then temporally processed: detrended, band-passed (from 0.017 Hz to 80% of the Nyquist frequency) with DC recovery, then normalized to percent changes based on blank periods. Regions of interest (ROIs) were defined by hand, referring to the monkey atlas [14].

For neuronal data, broadband signals were decimated by a factor of 3 and a principal component analysis (PCA)-based denoising method was applied to remove residual interference [11]. In summary, data were split into chunks of different segment/slice values and the mean changes in each chunk were subtracted. Then principal components correlated with gradient changes were projected out. After this clean-up step, the signal was processed in eight frequency bands (1–8, 8–12, 12–24, 24–40, 40–60, 60–100, 120–250 and 1000–3000 Hz, named δ/θ , α , β , γ_L , γ , γ_H , γ_{VH} and multiunit activity, respectively). Appropriate down-sampling and band-pass filtering (zero phase distortion by bidirectional processing) were used to avoid singularities of digital filtering. The signal was then converted into absolute amplitude, resampled to 250 Hz after the appropriate low-pass filtering and normalized to standard deviation units (SDU) based on blank periods. Frequency separation was based on results from information theoretical analysis [15]. Time-dependent FFT analysis (spectrograms) was also used and yielded the same results as those obtained by band-pass filtering. Discrete spike times were also extracted by windowing the high-passed waveform of the broadband signal with a threshold of 2.4 in SDU. Instantaneous spike rates were calculated in hertz by assigning the spike times in bins of 100 ms width.

2.4. Temporal kernel-based canonical correlation analysis

We used tkCCA to explore the dynamic profiles of the fMRI and neural signals. The method was developed recently and is described in detail elsewhere [9]. tkCCA maximizes the canonical correlation between the data by comparing kernels rather than the covariance matrices used in classical CCA [16], which are computationally impracticable due to the large number of voxels in fMRI. Maximization is performed as a whole, automatically taking into account various aspects such as frequency bands of the neural signal, as well as the spatial differences in the fMRI time series. This unique property of tkCCA clearly distinguishes it from standard correlation analysis, which simply computes similarities between neural signal(s) and each voxel time course individually without any global optimization.

We consider the neural data as $X \in \mathbb{R}^{M \times T}$ and fMRI data as $Y \in \mathbb{R}^{N \times T}$, where M denotes the number of neural bands, N denotes the number of fMRI voxels and T denotes the

number of samples in time. The tkCCA method finds filters which maximize the correlation between X and Y . The temporal dynamics of the coupling can be accounted for by looking at canonical correlations at different time lags. In other words, the data matrix \tilde{X} used for tkCCA contains all time-shifted versions of the data as additional dimensions like $\tilde{X} \in \mathbb{R}^{ML \times T}$, where L denotes the number of different lags. Now, the objective of tkCCA is:

$$\underset{\tilde{w}_x, w_y}{\operatorname{argmax}} \operatorname{Corr}(\tilde{w}_x^T \tilde{X}, w_y^T Y) \quad (1)$$

The method uses the kernels $K_{\tilde{X}} = \tilde{X}^T \tilde{X}$ and $K_{\tilde{X}} \tilde{X}^T \tilde{X}$, and the solution of KCCA can be computed by solving the generalized eigenvalue problem:

$$\begin{bmatrix} 0 & K_{\tilde{X}} K_Y \\ K_Y K_{\tilde{X}} & 0 \end{bmatrix} \begin{bmatrix} \alpha \\ \beta \end{bmatrix} = \rho \begin{bmatrix} K_{\tilde{X}}^2 + \lambda_{\tilde{X}} K_{\tilde{X}} & 0 \\ 0 & K_Y^2 + \lambda_Y K_Y \end{bmatrix} \begin{bmatrix} \alpha \\ \beta \end{bmatrix} \quad (2)$$

where $\lambda_{\tilde{X}}$ and λ_Y are regularization parameters that control the complexity of the solution. The resolved filters \tilde{w}_x, w_y can be interpreted as the contribution of each feature (e.g., band, lag, voxel). The projecting filter \tilde{w}_x can be reshaped into a $M \times L$ matrix, yielding a time-dependent multivariate filter $w_x(\tau)$. The stationary projection w_y can be considered the pattern in voxel space. We can use the result of tkCCA like a standard univariate cross-correlogram in order to compute a canonical cross-correlogram:

$$\rho(\tau) = \operatorname{Corr}(w_x(\tau)^T X, w_y^T Y) \quad (3)$$

Here, $w_x(\tau)$ denotes a weight vector for neural bands at a given time lag. Since CCA is inherently insensitive to the sign of the correlation, one always has to take into account both the canonical correlogram and the corresponding canonical variates $w_x(\tau)$ and w_y in order to interpret the tkCCA results. Positive and negative correlations between signals are encoded as the relative signs of the $w_x(\tau)$ elements. Here, we switched the signs such that the sum of w_y was positive. The typical processing time for the tkCCA on a computer (MATLAB 7.5, 3GHz Intel Xeon, 4GB RAM) for our data set (150 time points, ~2000 voxels and nine neural signals) was about 7 s.

In the present study, we used neural bands and BOLD signals from a defined ROI. Neural signals were resampled to match the sampling rate of the BOLD signal and then passed to the tkCCA algorithm. For comparison, the same data set was used with an averaged BOLD time course to apply standard correlation analysis for each frequency band. The system-identification toolbox of MATLAB was also used to estimate the impulse response function (HRF) from a univariate neural signal in each frequency band to a univariate BOLD signal which was simply the average time course in the chosen ROI. Spontaneous activities of

each neural band/channel and BOLD signal (average of the given ROI) were both resampled to 20 Hz, converted into S. D. units and correlation analysis was applied after pre-whitening (order of 5) to avoid pseudocorrelation between lower neural bands and BOLD signals. In the following we will refer to these univariately estimated impulse response functions as HRFs, unless stated otherwise.

3. Results

We performed simultaneous fMRI and neurophysiological recordings in V1 of anesthetized monkeys. To record neural activity, we used a multichannel electrode which was placed over the opercular part of V1 on the basis of information obtained from structural MR scans (Fig. 1A, top). The electrodes induced only limited susceptibility artifacts, showing little or no loss of BOLD signal around the tip. For data analysis, we used V1 regions (ROIs) determined on the basis of anatomical landmarks. In each session, test scans using full-field visual stimuli were carried out to ensure the existence of robust BOLD responses within the anatomically defined V1 regions (Fig. 1A lower). Following this mapping, spontaneous fluctuations of the neurophysiological and BOLD signals were recorded in 5–10 blocks, each with a duration of 5 min (Fig. 1B and 1C).

Consistent with our previous work [11,17], conventional correlation analysis showed that the BOLD activity around the tip of the electrode correlates with the overall underlying neural activity as measured with intracranial electrodes. During stimulus presentation, changes in neural activity were closely followed by changes in the BOLD signal. In contrast, during spontaneous activity increases in the γ range of the LFP and in the spiking activity occasionally failed to elicit changes in the BOLD response. We note here in passing that the BOLD signal, examined with the above-mentioned method, represents the average of all time courses within the selected ROIs. This average does not differentially weigh the contribution of individual voxels nor does it take into account the potential differences in their time lag [5]; it can therefore occasionally miss hemodynamic changes restricted to a subset of each ROI—a problem that could in principle be addressed by using the tkCCA method. What follows are results obtained using tkCCA and the degree to which this analysis provides us with further insights into neurovascular coupling.

Fig. 2 shows a representative example of tkCCA on simultaneously acquired neural and fMRI data without any visual stimulation. Fig. 2A displays the frequency–time filter estimated by the tkCCA and Fig. 2B, the optimal spatial filter for the fMRI time series. The right column of Fig. 2B depicts the calculated weights for each voxel superimposed on a typical anatomical scan, as shown in the left panels. The frequency–time matrix has higher weights in γ (γ_L , γ , γ_H and γ_{VH} , i.e., 40–250 Hz) and MUA ranges, at a time lag of about 5 s (Fig. 2A); neural activity

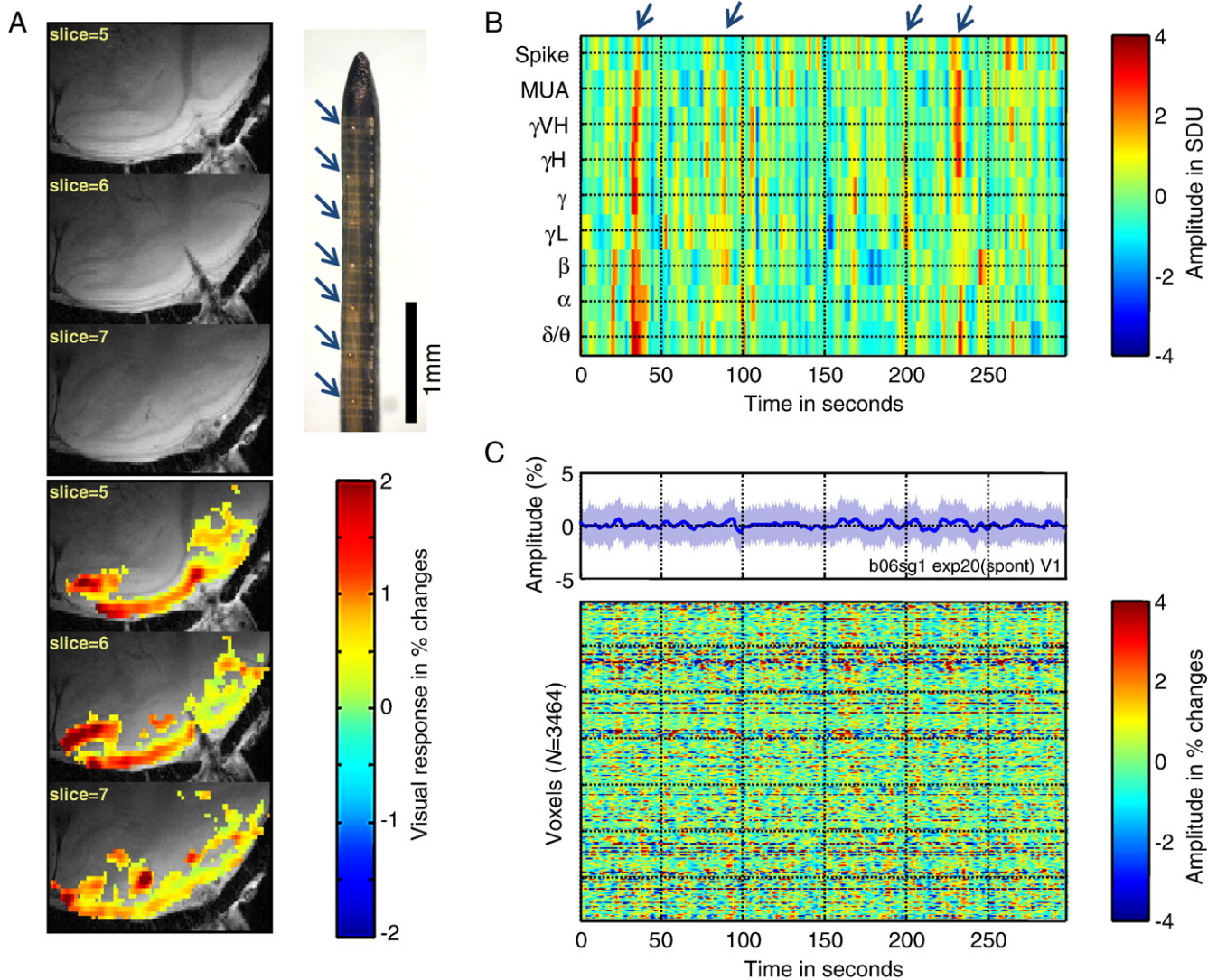


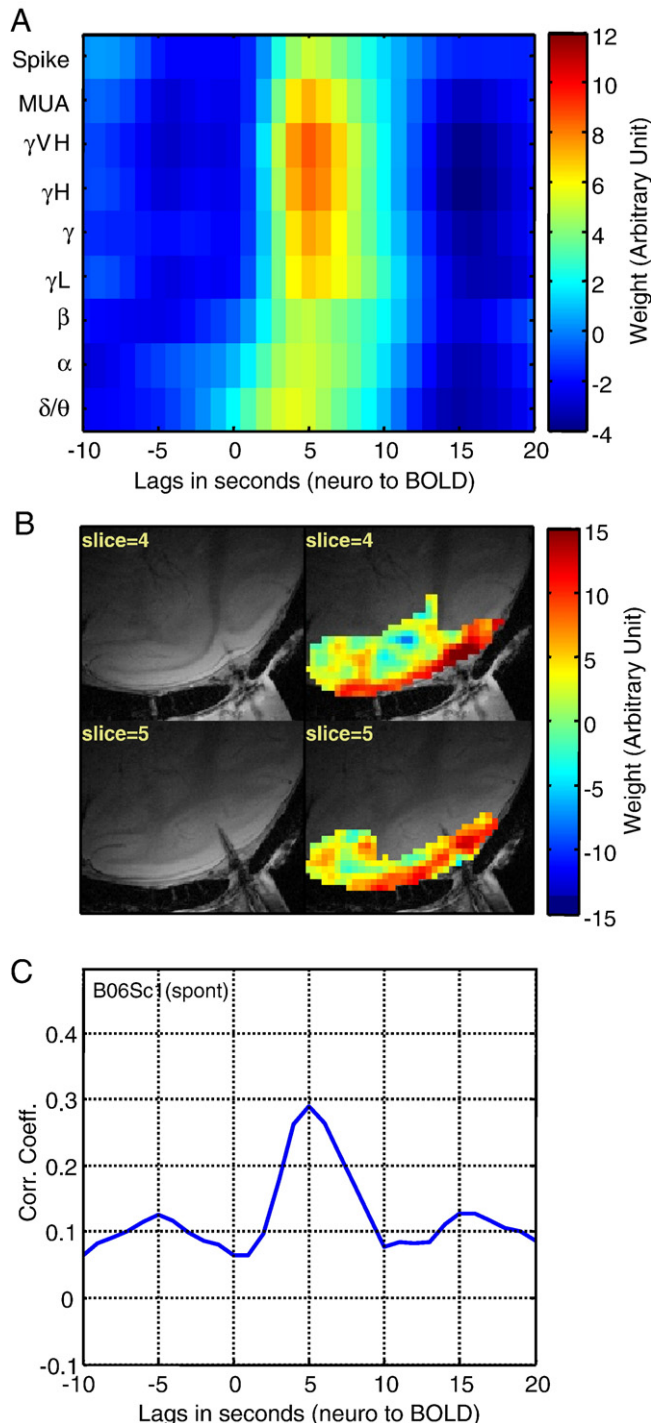
Fig. 1. Recording hardware, activation maps and analysis principles for combined physiology-fMRI experiments. (A) The upper column shows anatomical images and the multichannel electrode used in this study. Blue arrows represent positions of recording sites on the electrode; 7 out of 10 channels are visible. The lower column shows the BOLD responses ($P < .001$) tested by means of a full-field visual stimulus. Note the minimal susceptibility artifacts caused by the electrode; no distortions are evident in the activation map. (B) Spontaneous changes in the amplitude of different frequency bands. Depicted are the bands δ/θ , α , β , γ , γL , γH , γVH , MUA (multi-unit activity) with 1–8, 8–12, 12–24, 24–40, 40–60, 60–100, 120–250 and 1000–3000 Hz, respectively. Spikes were extracted by detecting zero crossings and thresholding the high-pass signal. Arrows show examples of synchronous γ and spiking activation. The entire frequency–time matrix was used for tkCCA. (C) Spontaneous changes in the BOLD signal in the regions of V1, defined on the basis of anatomical criteria in each slice. The upper trace shows the average time course of BOLD fluctuations from all voxels seen below.

in bands below 24 Hz (δ/θ , α , β bands) makes smaller contributions to the BOLD signal changes. The estimated optimal spatial filter (Fig. 2B), on the other hand, shows that voxels within the gray matter (red stripe) of V1 make a larger contribution to the maximized correlation between the neural and fMRI signals. In the present study the γ and MUA contributions were greater than those of spiking activity, which commonly represents a small group of cells. The strong contribution of the γ and MUA bands was observed in most cases (see also Fig. 3A), and it confirms previous results showing that the highest correlation between the neural and the BOLD responses occurred in the 30- to 140-Hz range of the neural signal in intracranial

recordings in the anesthetized monkey [11] and in human patients [18,19].

In order to compare tkCCA with conventional correlation analysis, we estimated the canonical correlogram as defined in Eq. (3). This canonical correlogram is similar to the univariate cross-correlogram, except that it is strictly positive. However, the right sign of correlation can be identified by looking at the signs of the projection coefficients (see Methods section). Much as with the correlogram computed in mass-univariate approaches, the peak of the correlogram was found at a lag of about 5 s, suggesting that, at least in area V1, the time-to-peak of the BOLD response occurs 5 s after the onset of neural activity.

The aforementioned temporal patterns were observed in most sessions. Fig. 3A shows the average weight matrix for the neural signals. For averaging, temporal filters were normalized in each session to the maximum value of the γ range weight. As in the example shown in Fig. 2A, the averaged filter for neural signals showed a greater contribution of the γ and MUA ranges. These larger weights also had a positive correlation to the BOLD signal with a delay of 4.4 ± 0.7 s (mean \pm S.D., $n=12$); this value is



consistent with the time-to-peak of the HRF reported previously [11,20–23].

In addition to the canonical correlogram, a single correlation coefficient was computed between neural and BOLD time series using all weights in the two filters; the mean value was 0.54 ± 0.18 (mean \pm S.D., $n=12$). Interestingly this coefficient was significantly higher ($P=0.0072$, two-sample t test) than that computed with traditional correlation analysis (0.39 ± 0.04 , $n=12$), for example, using averaging and convolution with fixed-width HRF [21]. The difference in correlation-strength between the tkCCA and HRF-based correlation analysis suggests that by taking into account the differential contribution of neural channels, lags and voxels, the former method substantially improves the measurement of dependencies between neural and BOLD activity.

Finally, we compared the frequency–time structure estimated with tkCCA with the HRFs estimated by considering each frequency band as an independent neural signal and the average of all ROIs time courses as the fMRI response. We used the standard system identification techniques to estimate the HRF. Specifically, both the neural and the fMRI signals were prewhitened with an AR model of the input (see methods and reference by Logothetis et al. [11]). Covariance analysis was subsequently applied and the positive lags were taken as the HRF of the neurovascular system. Fig. 4A shows averaged HRFs of each neural band ($n=12$) obtained by such a method. As observed in Fig. 4A and B, neural fluctuations in the γ (γ L, γ , γ H and γ VH) and MUA ranges have a larger impact on BOLD than other frequency bands. The amplitude of the HRF from γ was about two times larger than that from MUA or spikes. Time to peak was between 4 and 5 s. To evaluate the results quantitatively, we fitted a low-order Gamma function [21] to the estimated HRF at each frequency band, with fitting parameters including the values of amplitude and time to peak. As shown in Fig. 5A, the time to peak did not differ significantly between tkCCA and HRF; all frequency bands showed

Fig. 2. Contribution (weights) of different frequency bands at different time lags in the temporal dynamics of BOLD within the selected V1-ROI in a sample session (here, B06Sc1). (A) Optimal frequency–time filter for neuronal data computed by tkCCA. The x-axis shows the time lags of the band-limited neural signal, that is, time shifts, equal to the volume repetition time of the MR images. Displayed are time shifts in the range of –10 to 20 s. The greater weights (red) in the middle of the plot indicate that changes in activity in the 24- to 250-Hz range contribute maximally to the BOLD signal alterations occurring approximately 5 s later. (B) The left column shows the anatomical images and the right the optimal spatial filter for the V1 fMRI data computed by tkCCA; the weights are superimposed on the anatomical scans, showing the locations in V1 that are best (red) correlated with the global neural activity. (C) Canonical correlogram between the neural and the BOLD time courses. For each lag the weights of each band are used to calculate a weighted average of the neural response; the latter is subsequently correlated with the weighted average of MRI time series, and the correlation coefficient is plotted as a function of time lag. Peak correlations are observed at a lag of approximately 5 s.

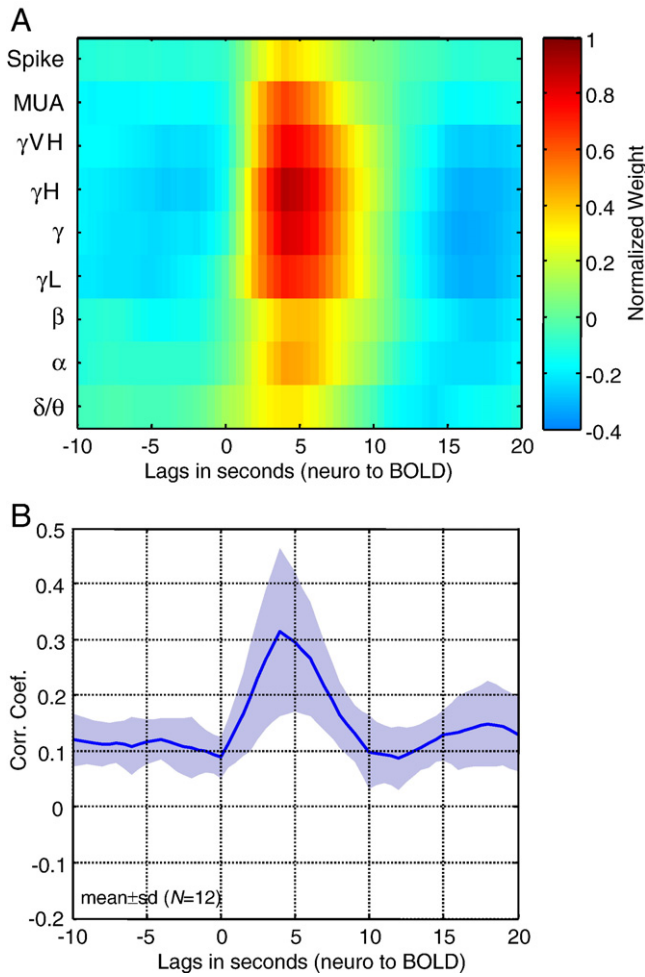


Fig. 3. Averaged temporal dynamics from tkCCA results for all sessions. (A) Average frequency–time filter for neural signals ($n=12$). The filter of each session was normalized to the maximum weight of the γ band before averaging. Overall, the γ range activities and MUA appear to have the higher weights during spontaneous activity. (B) Average of canonical correlogram between neural and BOLD data ($n=12$); conventions as in Fig. 2.

similar values. On average, values acquired with tkCCA and HRF were 4.9 ± 0.9 and 4.8 ± 0.1 s, respectively (mean \pm S.D., computed at γ range, $n=12$). The amplitude profiles of tkCCA and HRF were also similar to each other (Fig. 5B). They had a bell shape, peaking at the γ (γ_L , γ , γ_H and γ_{VH} , i.e., 40–250 Hz) to MUA range. A minor difference was seen in the lower frequency range (δ/θ , α and β , i.e., 1–24 Hz), where tkCCA showed a small contribution to the BOLD fluctuation, whereas the HRF of that band did not. One possible explanation for this difference is that without explicit prewhitening tkCCA might be more sensitive to autocorrelations in either data source than the univariate approach. When the BOLD response contains a component which is simply a time-shifted version of the neural response at a lower frequency range, the covariance analysis might fail to compute the HRF as a result of the prewhitening, which might leave no significant residual.

4. Discussion

We have shown here that tkCCA can be successfully applied to the analysis of combined physiological and fMRI data, and that it might provide further insights into the spatiotemporal dynamics of the neurovascular correlation from spontaneous fluctuations. In general, the present findings are in accordance with those reported in previous studies investigating the neurovascular coupling in the same cortical region under conventional visual stimulation in monkeys [11,17,24–26]. During spontaneous activity, both LFP and spiking activity correlated with the BOLD signal,

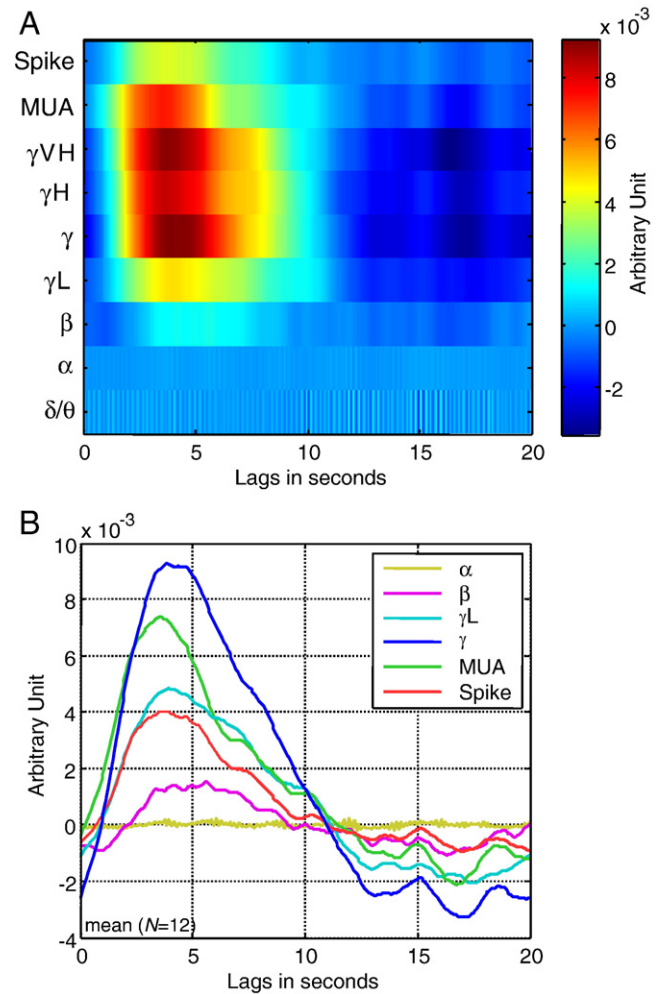


Fig. 4. Averaged HRFs computed for each neural activity at different frequency bands. (A) The average HRFs ($n=12$) were computed using standard system identification methods, that is, by applying covariance analysis and taking the positive lags as the impulse response of the system. The same data set as in Fig. 3 was used. The neural fluctuations of each frequency band and the averaged BOLD signal around the recorded site were prewhitened and then used to compute the transfer function (impulse response function) from neural to BOLD signal. Neural fluctuations in the γ and MUA ranges have a larger amplitude than other frequency bands. (B) Plot of averaged HRFs for α , β , γ_L , γ , MUA and spike ranges. Amplitude of the HRF in the γ range of LFPs was about two times larger than those from MUA or spike ranges. Time to peak lies between 4 to 5 s.

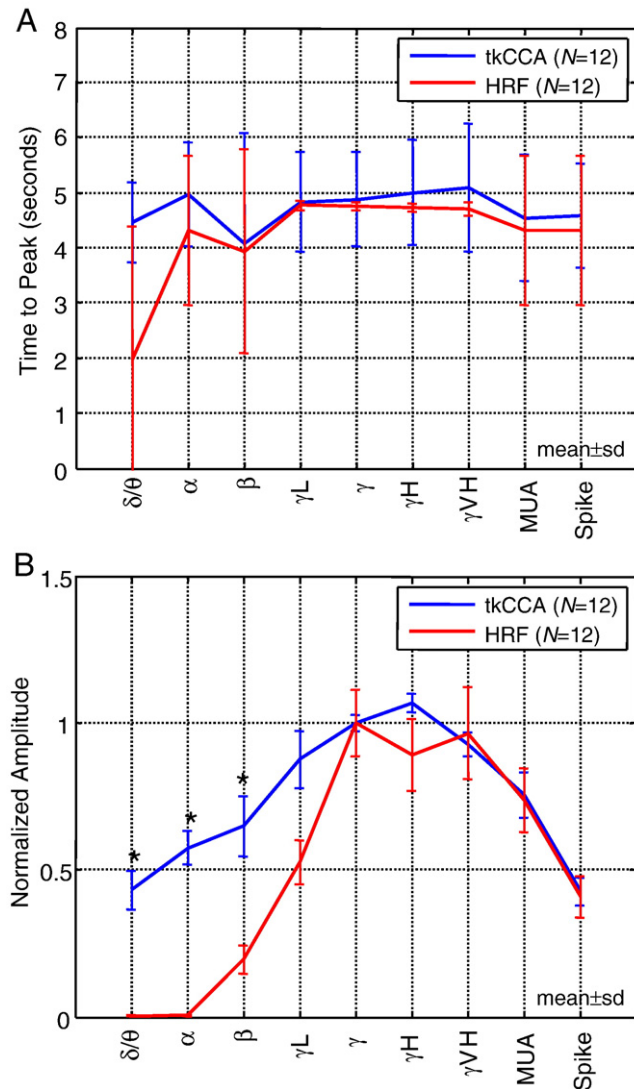


Fig. 5. Comparison between results from tkCCA and HRF. (A) Comparison of time to peak between temporal filter of tkCCA and HRF ($n=12$). There was no significant difference between tkCCA and HRF values. (B) Comparison of peak amplitudes between tkCCA and HRF ($n=12$). Values were normalized to the value of the γ range for each session. “*” represents the significant difference between tkCCA and HRF values ($P<.01$, two-sample t test).

and the γ ranges of LFPs contributed more than other bands do. With respect to the neuronal contribution to the BOLD signal, both uni- and multivariate methods yielded similar results, but tkCCA provided useful additional information, namely, a concurrent spatial pattern for fMRI data that depicts which part of the brain correlated better or worse with the neural data. The spatial correlation pattern revealed a larger contribution of voxels localized in the gray matter of the opercular V1, including the recording sites. These results demonstrate the reliability and the efficacy of tkCCA in investigating neurovascular coupling in the frequency–time domain for neural data and as well as the spatial pattern of coupling in fMRI space.

tkCCA computes two weight filters for the neural and the BOLD signals. The method assigns higher values to

elements which contribute to a higher canonical correlation between the two signals overall. In other words, the method detects features in the frequency–time space of the neural signal as well as in the spatial space in the fMRI data. The optimization process runs without assumptions about the transfer function of the neurovascular system. In this sense, tkCCA differs from classic correlation analysis and regression analysis, which assume and use convolution of models with the known hemodynamic kernel. Indeed, the correlation coefficients computed by tkCCA using optimized weights were higher than those obtained with a fixed-width kernel, indicating that tkCCA detects individual differences in features in each dimensional space of the neuronal and fMRI data. It may also be interesting to know how we can give a bias to tkCCA based on appropriate prior knowledge, for example, an anatomical constraint. While in the present study we used generic regularization in the maximization process for the correlation, further pragmatic investigations are required to examine the potential for improvement from using physiological biases.

The frequency–time filter selected by tkCCA and the HRF at different neural bands showed similar patterns, demonstrating the validity of the new method for use with combined fMRI and neurophysiological recordings. During spontaneous activity, neural changes in the γ and MUA ranges made a greater contribution to the BOLD fluctuations than others. The observed profiles in the frequency–time filter are consistent with previous observations showing that LFP are closely correlated to the BOLD signals during visually stimulated period in non-human primates [11,17].

In addition to the frequency–time structure of correlation, tkCCA yields the spatial filter for the BOLD time courses. The spatial filter for fMRI data showed higher coupling near the electrode and the large spread of the coupling over the opercular V1 over a range of several centimeters. We observed a relatively large spatial extent of correlated voxels, which may stem from the fact that widespread correlations are often observed during spontaneous conditions as opposed to stimulus-based conditions [27,28]. To apply tkCCA, we downsampled the neural signals to match the fMRI time courses. This process essentially operates like low-pass filtering, limiting the band width as low as the fMRI data. As a result, tkCCA could detect correlations to very slow components of each neural band, which are known to spread as measured by neurophysiological recordings [29].

While the observed aspects in each of the time-frequency and the spatial correlations are merely a confirmation of previous studies, the spatial filters computed by tkCCA reveal the correlation structure in V1 that maximizes the neurovascular dependencies. This can provide valuable insights into the functional connectivity of V1. To date, most fMRI connectivity studies have had to rely entirely on unsupervised methods that use only fMRI data [30–33] or supervised methods that correlate BOLD data with stimulus time series (including some model assumptions about the HRF). The proposed method in combination with the simultaneous

recordings of neural activity offers a purely data-driven approach to the multivariate analysis of neurovascular coupling mechanisms. In other words, it does not make any a priori assumptions about the HRF, the frequency profile or spatial dependencies, but instead directly estimates these parameters from the data. This means that results generated with tkCCA are not affected by preassumed HRF, which is likely to be different in each brain area due to anatomical differences or variations in sensitivity due to neuromodulatory inputs. In addition, an important advantage of the method is that both filters are estimated concurrently to maximize the correlation between the signals, implying that functional connectivity revealed by tkCCA represents unbiased signal correlations in both time-frequency and spatial domains. This unique property of tkCCA will probably allow us to address further aspects of functional connections, in particular by comparing the BOLD signals in each brain region with neural responses recorded from one area.

Acknowledgments

We would like to thank M. Lindig and D. Ipek for technical support; S. Weber and K.H. Hofmann for their fine mechanics wizardry; J. Werner for computer assistance; and Dr. K. Whittingstall for discussions of an earlier manuscript. This work was supported by the Max Planck Society and has been supported as a Bernstein Cooperation (German Federal Ministry of Education and Science), Foerderkennzeichen 01 GQ 0711.

References

- [1] Ogawa S, Lee TM, Nayak AS, Glynn P. Oxygenation-sensitive contrast in magnetic resonance image of rodent brain at high magnetic fields. *Magn Reson Med* 1990;14:68–78.
- [2] Logothetis NK. The neural basis of the blood-oxygen-level-dependent functional magnetic resonance imaging signal. *Philos Trans R Soc Lond B Biol Sci* 2002;357:1003–37.
- [3] Logothetis NK, Wandell BA. Interpreting the BOLD signal. *Annu Rev Physiol* 2004;66:735–69.
- [4] Logothetis NK. What we can do and what we cannot do with fMRI. *Nature* 2008;453:869–78.
- [5] Aguirre GK, Zarahn E, D'Esposito M. The variability of human, BOLD hemodynamic responses. *Neuroimage* 1998;8:360–9.
- [6] Chang C, Thomason ME, Glover GH. Mapping and correction of vascular hemodynamic latency in the BOLD signal. *Neuroimage* 2008;43:90–102.
- [7] Lange N, Strother SC, Anderson JR, Nielsen FÅ, Holmes AP, Kolenda T, et al. Plurality and resemblance in fMRI data analysis. *Neuroimage* 1999;10:282–303.
- [8] Norman KA, Polyn SM, Detre GJ, Haxby JV. Beyond mind-reading: multi-voxel pattern analysis of fMRI data. *Trends Cogn Sci* 2006;10:424–30.
- [9] Bießmann F, Meinecke FC, Gretton A, Rauch A, Rainer G, Logothetis NK, Müller KR. Temporal kernel CCA and its application in multimodal neuronal Data Analysis. *Mach Learn* 2009. Published online DOI: 10.1007/s10994-009-5153-3.
- [10] Sheinberg DL, Logothetis NK. Noticing familiar objects in real world scenes: the role of temporal cortical neurons in natural vision. *J Neurosci* 2001;21:1340–50.
- [11] Logothetis NK, Pauls J, Augath M, Trinath T, Oeltermann A. Neurophysiological investigation of the basis of the fMRI signal. *Nature* 2001;412:150–7.
- [12] Oeltermann A, Augath MA, Logothetis NK. Simultaneous recording of neuronal signals and functional NMR imaging. *Magn Reson Imaging* 2007;25:760–74.
- [13] Logothetis NK, Murayama Y, Augath M, Steffen T, Werner J, Oeltermann A. How not to study spontaneous activity. *Neuroimage* 2009;45:1080–9.
- [14] Saleem KS, Logothetis NK. A combined MRI and histology atlas of the rhesus monkey brain in stereotaxic coordinates. London, Burlington, MA: Academic Press (Elsevier Limited); 2007. p. 326.
- [15] Belitski A, Gretton A, Magri C, Murayama Y, Montemurro MA, Logothetis NK, et al. Low-frequency local field potentials and spikes in primary visual cortex convey independent visual information. *J Neurosci* 2008;28:5696–709.
- [16] Hotelling H. Relations between two sets of variates. *Biometrika* 1936;28:321–77.
- [17] Goense JBM, Logothetis NK. Neurophysiology of the BOLD fMRI signal in awake monkeys. *Curr Biol* 2008;18:631–40.
- [18] Mukamel R, Gelbard H, Arieli A, Hasson U, Fried I, Malach R. Coupling between neuronal firing, field potentials, and fMRI in human auditory cortex. *Science* 2005;309:951–4.
- [19] Nir Y, Fisch L, Mukamel R, Gelbard-Sagiv H, Arieli A, Fried I, et al. Coupling between neuronal firing rate, gamma LFP, and BOLD fMRI is related to interneuronal correlations. *Curr Biol* 2007;17:1275–85.
- [20] Friston KJ, Frith CD, Turner R, Frackowiak RSJ. Characterizing evoked hemodynamics with fMRI. *Neuroimage* 1995;2:157–65.
- [21] Cohen MS. Parametric analysis of fMRI data using linear systems methods. *Neuroimage* 1997;6:93–103.
- [22] Glover GH. Deconvolution of impulse response in event-related BOLD fMRI. *Neuroimage* 1999;9:416–29.
- [23] Buxton RB, Uludağ K, Dubowitz DJ, Liu TT. Modeling the hemodynamic response to brain activation. *Neuroimage* 2004;23 (Suppl 1):S220–33.
- [24] Rauch A, Rainer G, Logothetis NK. The effect of a serotonin-induced dissociation between spiking and perisynaptic activity on BOLD functional MRI. *Proc Natl Acad Sci U S A* 2008;105:6759–64.
- [25] Kayser C, Kim M, Ugurbil K, Kim DS, König P. A comparison of hemodynamic and neural responses in cat visual cortex using complex stimuli. *Cereb Cortex* 2004;14:881–91.
- [26] Maier A, Wilke M, Aura C, Zhu C, Ye FQ, Leopold DA. Divergence of fMRI and neural signals in V1 during perceptual suppression in the awake monkey. *Nat Neurosci* 2008;11:1193–200.
- [27] Bartels A, Zeki S. Brain dynamics during natural viewing conditions—a new guide for mapping connectivity in vivo. *Neuroimage* 2005;24:339–49.
- [28] Nauhaus I, Busse L, Carandini M, Ringach DL. Stimulus contrast modulates functional connectivity in visual cortex. *Nat Neurosci* 2009;12:70–6.
- [29] Leopold DA, Murayama Y, Logothetis NK. Very slow activity fluctuations in monkey visual cortex: implications for functional brain imaging. *Cereb Cortex* 2003;13:422–33.
- [30] Biswal B, Yetkin FZ, Haughton VM, Hyde JS. Functional connectivity in the motor cortex of resting human brain using echo-planar MRI. *Magn Reson Med* 1995;34:537–41.
- [31] Lowe MJ, Mock BJ, Sorenson JA. Functional connectivity in single and multislice echoplanar imaging using resting-state fluctuations. *Neuroimage* 1998;7:119–32.
- [32] Cordes D, Haughton VM, Arfanakis K, Carew JD, Turski PA, Moritz CH, et al. Frequencies contributing to functional connectivity in the cerebral cortex in “resting-state” data. *AJNR Am J Neuroradiol* 2001;22:1326–33.
- [33] Friston K. Causal modelling and brain connectivity in functional magnetic resonance imaging. *PLoS Biol* 2009;7:e33.